

The seismic noise environment of Europa

M. P. Panning^{1*}, S. C. Stähler^{2†}, H.-H. Huang^{3‡}, S. D. Vance⁴, S. Kedar⁴, V. C. Tsai³, W. T. Pike⁵, R. D. Lorenz⁶

¹Dept. of Geological Sciences, Univ. of Florida, Gainesville, Florida, USA

²Dept. of Earth and Environmental Sciences, Ludwig-Maximilians-Universität, Munich, Germany

³Seismological Laboratory, California Institute of Technology, Pasadena, California, USA

⁴Jet Propulsion Laboratory, California Institute of Technology, Pasadena, California, USA

⁵Department of Electrical and Electronic Engineering, Imperial College, London, United Kingdom

⁶Space Exploration Sector, Johns Hopkins Applied Physics Laboratory, Laurel, Maryland, USA

Key Points:

- Ambient seismic noise due to tidal cracking in the ice on Europa is estimated
- Noise is modeled with a Gutenberg-Richter relationship using numerical wave propagation
- Estimated signal and noise suggest a high-frequency geophone will not be adequate for a landed mission

*now at Jet Propulsion Laboratory, California Institute of Technology, Pasadena, California, USA

†now at Institute of Geophysics, ETH Zürich, Zürich, Switzerland

‡now at Institute of Earth Sciences, Academia Sinica, Taipei, Taiwan

Corresponding author: M. P. Panning, mpanning@ufl.edu

Abstract

Seismic data will be a vital geophysical constraint on internal structure of Europa if we land instruments on the surface. Quantifying expected seismic noise on Europa is an important consideration for instrument and mission design. Noise will likely include cracking in the ice shell and turbulent motion in the oceans. We define a range of models of seismic activity in Europa’s ice shell by assuming each model follows a Gutenberg-Richter relationship with varying parameters. A range of cumulative seismic moment release between 10^{16} and 10^{18} Nm/yr is defined by scaling tidal dissipation energy to tectonic events on the Earth’s moon. Random catalogs are generated and used to create synthetic noise records through numerical wave propagation in thermodynamically self-consistent models of the interior structure of Europa. Spectral characteristics of the noise are calculated by determining probabilistic power spectral densities of the synthetic records. While the range of seismicity models predicts noise levels that vary by 80 dB, we show that most noise estimates are below the self-noise floor of high-frequency geophones, but may be recorded by more sensitive instruments. Such instruments appear likely to be able to record signals from the largest events expected during a window of a few weeks. Noise records may allow for constraints on interior structure through autocorrelation. Models of seismic noise generated by pressure variations at the base of the ice shell due to turbulent motions in the subsurface ocean may also generate observable seismic noise.

1 Introduction

Europa is a fascinating target which is likely to be a focus of future planetary science missions. Observations from the Voyager and Galileo missions [Kohlhase and Penzo, 1977; Russell, 2012] and Earth-based observations reveal a young, fractured icy surface [Zahnle *et al.*, 2003] with magnetic signals that indicate a global subsurface ocean [Kivelson *et al.*, 2000]. The presence of liquid water makes the moon a prime target for astrobiological investigations, leading to multiple future missions in the planning stages, including the Europa Clipper from NASA [Phillips and Pappalardo, 2014], the JUICE mission from ESA [Grasset *et al.*, 2013], and a proposed Europa lander mission [Hand *et al.*, 2017].

While coarse information about subsurface structure of planetary bodies can be gleaned from gravity and magnetic observations from orbital and Earth-based observations, such models are generally quite non-unique. Other geophysical observations will be required in order to determine more precise details, such as thickness of the ice shell, depth to the ocean bottom, and any other details of structure beneath the ocean. Orbital ice penetrating radar measurements have long been proposed to look for the depth to Europa’s ocean [e.g. Chyba *et al.*, 1998]. Scattering in an impact garden or tidally fractured regolith may cause this to be a problematic observation [Eluskiewicz, 2004], although more recent studies suggest the scattering may not be so problematic [Aglyamov *et al.*, 2017]. If a lander is sent to Europa [Hand *et al.*, 2017], a seismometer would provide an important complement to radar observations. In fact, seismology has been the primary geophysical technique constraining the detailed structure of the Earth’s interior. Several previous studies have identified seismic signals ranging across a broad frequency band with the potential to provide important subsurface structural constraints on Europa [Kovach and Chyba, 2001; Lee *et al.*, 2003; Panning *et al.*, 2006], while seismic investigations also present the opportunity to observe other signals of activity in Europa’s ice shell and ocean that could have relevance to astrobiological investigations [Vance *et al.*, 2017a].

Before a seismometer is sent, however, it is important to attempt to quantify instrument requirements as well as possible. Obviously, an instrument needs to be sensitive enough to record the desired signals, whether these be body waves reflecting from the base of the ice shell and ocean [e.g. Lee *et al.*, 2003] or other longer-period signals [Kovach and Chyba, 2001; Panning *et al.*, 2006], but it is also important to estimate the amplitude of the ambient noise. This noise estimate informs mission planners of likely signal-to-noise ratios and sets

an important baseline for instrument sensitivity. Designing an instrument that is sensitive to signals orders of magnitude below the ambient noise floor is inefficient, but being able to record the noise floor can provide important science return on its own.

On Earth, the majority of the energy of the ambient noise field originates in the oceans, and analyzing it in the “microseismic band” (at periods roughly between 5 and 20 seconds) provides important constraints on wave interactions relatively near the shore [e.g. *Longuet-Higgins*, 1950], while signals due to infragravity waves excited by ocean storms cause continuous oscillations of the whole Earth at much longer periods [e.g. *Rhie and Romanowicz*, 2004]. Constraining the amplitudes and frequency characteristics of the noise therefore can give us important constraints on active processes occurring on a planetary scale. Following work looking at correlation of noise in event codas producing signals that approximate the seismic response between two stations [*Campillo and Paul*, 2003], noise records on Earth have also been extensively used in the last decade and a half to generate useful signals to constrain internal structure.

On Europa, we do not yet have any direct constraints on the seismic noise characteristics, but it is reasonable to hypothesize that such noise will be primarily generated by a combination of widespread ice-tectonic events (i.e. tidal cracking) within the ice shell and motions of the subsurface ocean. The energy source for both types of noise would be tidal deformation due to the slightly elliptical orbit of Europa around Jupiter. There is observational evidence for Hubble Space Telescope imaging of transient plumes of water vapor [*Roth et al.*, 2014] which suggests that opening and closing of cracks is ongoing today, and is controlled by tides [*Rhoden et al.*, 2015]. Further observations recently confirmed the plumes [*Sparks et al.*, 2017] and suggested they may be correlated with a thermal anomaly associated with tidal friction and/or access to the internal ocean.

In this study, we propose to produce quantitative estimates of the seismic noise due to widespread small ice-tectonic events, which is a problem amenable to careful quantification with a small number of assumed properties of Europa using available seismic modeling tools. We also look at an initial estimate of possible noise due to one model of turbulent flow in Europa’s ocean [*Soderlund et al.*, 2014], although further work on this noise source will be important.

2 Modeling tidal cracking events with a Gutenberg-Richter relationship

The slightly elliptical orbit of Europa around Jupiter causes tidal stresses that vary diurnally with amplitudes of ~ 100 kPa [e.g. *Hoppa et al.*, 1999]. This stress has been modeled as sufficient to induce fracturing extending 10’s of meters into the ice shell [*Lee et al.*, 2003]. In addition, some surface observations are used to argue for non-synchronous rotation of Europa [e.g. *Bills et al.*, 2009, for further details], and such motions could cause larger stress values, possibly exceeding 1 MPa [e.g. *Hurford et al.*, 2007; *Beuthe*, 2015]. Such larger stresses could cause cracking extending several kilometers into the ice shell [*Lee et al.*, 2005], which would generate significant seismic energy release.

Rather than attempting to model the distribution of ice-cracking events through detailed stress modeling, which depends strongly on many assumptions such as ice rheology, porosity, and brine content, we choose instead to use a simple statistical model to determine seismic energy release due to ongoing cracking events in the European ice shell. Following work by *Golombek et al.* [1992] for modeling seismicity of Mars, we choose to assume seismicity in Europa’s ice shell will follow a Gutenberg-Richter relationship [*Gutenberg and Richter*, 1944], which is typically written as a log-linear relationship between the number of events observed greater than or equal to a particular earthquake magnitude,

$$\log N(M_W) = a - bM_W, \quad (1)$$

where $N(M_W)$ is the number of events greater than or equal to moment magnitude M_W , and a and b are empirically defined parameters which are fit to a particular seismicity catalog.

Moment magnitude can be related to the seismic moment, M_0 , of a particular seismic event by the definition of M_W [Kanamori, 1977],

$$\log M_0 = 1.5M_W + 9.1, \quad (2)$$

and so *Golombek et al.* [1992] chose to write the Gutenberg-Richter relationship in an equivalent form as

$$N(M_0) = AM_0^{-B}, \quad (3)$$

where A and B are empirical parameters, which can be related to a and b by substitution from equation 2 into equation 1 to obtain $a = \log A - 9.1B$ and $b = 1.5B$.

If we assume seismicity on Europa will follow such a relationship (as is true for observed catalogs on the Earth and the Moon), expected numbers of events of any size can be calculated simply by specifying physical parameters that constrain the parameters A and B . *Golombek et al.* [1992] showed that these can be uniquely determined by specifying the cumulative seismic moment released per year, ΣM_0 , the maximum event size, M_0^* , and a value for b , which specifies the slope in the Gutenberg-Richter relationship, where the cumulative seismic moment and maximum event size can be related to A and B by the relationship

$$\Sigma M_0 = \frac{AB}{1-B} (M_0^*)^{1-B}. \quad (4)$$

While some variation in b values is observed in different seismic catalogs, all Earth catalogs generally have values that vary between ~ 0.7 and ~ 1.3 [Frolich and Davis, 1993], and so we choose to simply assume $b = 1$ for all catalogs we develop in this study, leaving us only to define the cumulative moment release and maximum event size.

We consider a range of options for the cumulative moment release estimate. A reasonable starting point for such an estimate would be to scale it to our only available planetary catalog aside from the Earth. Based on Apollo data, lunar seismicity is described by a cumulative seismic moment release of approximately 10^{15} Nm/yr [Oberst, 1987]. While there are multiple models for the driving energy of lunar seismicity, tidal periodicities in the occurrence rate [e.g. *Lammlein et al.*, 1974] suggest an important role for tidal dissipation energy in driving quakes. The dissipated tidal energy in the moon is estimated at 1.36 GW [Williams et al., 2001], while the dissipated energy in the ice shell of Europa has been estimated from 630 GW up to a few thousand GW [Tobie et al., 2003; Hussmann and Spohn, 2004; Vance et al., 2007], which is larger by approximately 3 orders of magnitude. Based on this, it is reasonable to expect cumulative moment release on Europa to significantly exceed that of the Earth's moon. However, it is likely an oversimplification to simply assume a linear scaling. For example, while brittle fracture leading to seismic energy release is likely in the upper portion of the icy shell [e.g. *Lee et al.*, 2003, 2005], the ice will likely be ductile at greater depths and higher temperatures, which means that energy dissipated at these depths is unlikely to produce seismic moment release. Based on spacings of geologic features, the brittle-ductile transition on Europa has been placed at a depth of approximately 2 km [e.g. *Pappalardo et al.*, 1999], meaning that the brittle portion of the shell would make up anywhere from several percent of the total volume for a thick shell to several tens of percent of the volume of a thin shell, which would suggest a corresponding reduction to simple linear scaling from the Earth's moon. Based on these considerations, we make an initial approximation that activity levels will be 1 to 3 orders of magnitude above that of the moon, leading to a range of 10^{16} to 10^{18} Nm/yr.

Nimmo and Schenk [2006] argue based on observed surface faulting in regions with Galileo data of sufficient resolution that observed faulting corresponds to a seismic moment magnitude of M_W 5.3, assuming a low shear modulus of the ice due to regolith development. If the shear modulus of the ice is closer to that of unfractured ice, this increases to a magnitude of $\sim M_W$ 6 [Panning et al., 2006]. Given that only a limited portion of the surface was investigated, this suggests the maximum event size should be at least M_W 6. With a b value

Table 1. Model parameters for seismicity models

Model	ΣM_0 (Nm)	M_0^* (Nm)
A	10^{16}	$10^{19.5}$
B	10^{16}	10^{18}
C	10^{18}	$10^{19.5}$
D	10^{18}	10^{18}
Preferred	10^{17}	$10^{18.5}$

of 1, there are an order of magnitude fewer events for each unit increase in magnitude, however a unit increase in magnitude corresponds to an increase in energy by a factor of ~ 30 . This means the largest events dominate the cumulative moment release, and so a larger maximum event size implies relatively fewer of the frequent small events most likely to be observed by a short duration surface landed experiment. This seems like a counter-intuitive result, as there is a general expectation that the maximum event size in a particular catalog and the cumulative moment release should be correlated. Likely, such a correlation is to be expected in most settings; however, there is no explicit physical relationship defining how such a correlation should be defined. Even if we could define such a relationship, we would expect some variance between catalogs in how closely correlated the maximum event size would be with the cumulative moment release. Therefore, we choose to consider a range of maximum event size between M_W 6 ($\sim 10^{18}$ Nm) and a more conservative estimate of $10^{19.5}$ Nm such as that used by *Golombek et al.* [1992] for Mars based on the maximum observed intraplate oceanic earthquakes on Earth.

Given this range of estimates for cumulative moment release, we choose to define 5 candidate models of Gutenberg-Richter parameters to describe the activity of ice-tectonic events in Europa’s ice shell (fig. 1). We define 4 end member models with either low (10^{16} Nm/yr; models A and B) or high (10^{18} Nm/yr; models C and D) cumulative moment release, and either a large ($10^{19.5}$ Nm; models A and C) or small (10^{18} Nm; models B and D) maximum event size (table 1). Finally we defined a “preferred” model with parameters between the end members ($\Sigma M_0 = 10^{17}$ Nm and $M_0^* = 10^{18.5}$ Nm). Figure 1A displays the statistics of random 1-week realizations of these catalog parameters. Theoretical Gutenberg-Richter relationships would make straight lines on these plots, but a random realization causes some variation around these straight lines, particularly near the small number of large events. Each catalog is realized by calculating a probability of occurrence of each event size per second, and then creating a catalog by comparing these probabilities to random numbers generated for a desired length of time (fig. 1B). We can then use these catalogs to generate synthetic long-duration seismic records, provided we also randomly assign location and source mechanism characteristics to each event, as discussed in section 4.

3 Europa structure models

Accurately modeling potential Europa noise signals relies also on correctly characterizing the seismic wave propagation from modeled noise sources. For this, we need realistic structure models that detail elastic properties, density, and anelastic attenuation structure. *Vance et al.* [2017b] have produced a tool for building models of icy ocean worlds that are thermodynamically self-consistent, and include up-to-date thermodynamic properties for ices, saline oceans, as well as the rocky interior and iron core of Europa. Radial structures are computed as per *Vance et al.* [2014], with self-consistent ice and ocean thermodynamics, using boundary conditions of surface and ice-ocean interface temperature. Thermodynamics for rock have been added as per *Cammarano et al.* [2006], with updates to account for rock porosity, mineral hydration, and the presence of Na-bearing minerals. All models

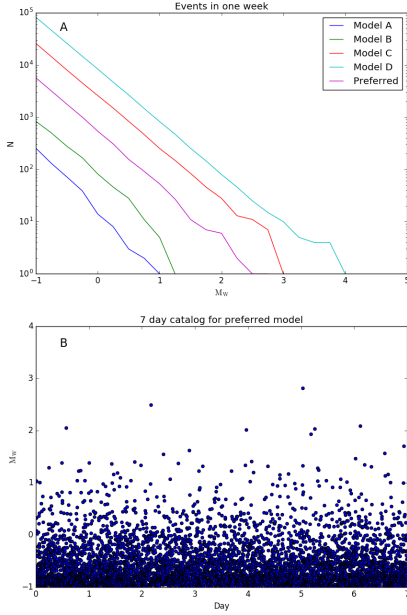


Figure 1. (A) Plotted Gutenberg-Richter relationships for random one-week realizations of 5 different seismicity models described in table 1. (B) Plot of one week of randomly realized events for the “preferred” model.

are designed to match the observations of a bulk density of $2989 \pm 46 \text{ kg m}^{-3}$ and normalized moment of inertia of 0.346 ± 0.005 [Schubert *et al.*, 2004]. All modeling tools are freely available via GitHub (<http://github.com/vancesteven/PlanetProfile>).

Temperature profiles can be tuned to produce different ice shell thicknesses. It is also possible to consider a range of internal compositions and temperature profiles for the interior below the ocean, but we only explore differences in ice shell thickness in this study (fig. 2). Previous modeling showed that observable seismic signals for sources located within the ice shell are dominated by the structure of the ice shell and have little sensitivity to structure below the ocean [Panning *et al.*, 2006]. For this study, we consider two different ice shell thicknesses, 5 and 20 km. Ice shell thickness has a very strong influence on the character of the surface waves, which grade from relatively non-dispersive Rayleigh waves to flexural waves at a characteristic frequency that depends on the thickness. There are also guided SV waves in the ice shell [Crary waves, Crary, 1954] that have characteristic frequency content that depends strongly on ice shell thickness. While ice shells thicker than 20 km are possible, these two values roughly bracket a reasonable range to constrain how overall noise characteristics may vary with thickness.

Amplitudes also depend on the attenuation structure of the model. For initial estimation, we followed the approach of Cammarano *et al.* [2006] to obtain temperature and frequency dependent estimates of shear quality factor, Q_μ with the expression

$$\frac{Q_\mu}{\omega^\gamma} = B_a \exp\left(\frac{\gamma H(P)}{RT}\right) \quad (5)$$

$$H(P) = g_a T_m, \quad (6)$$

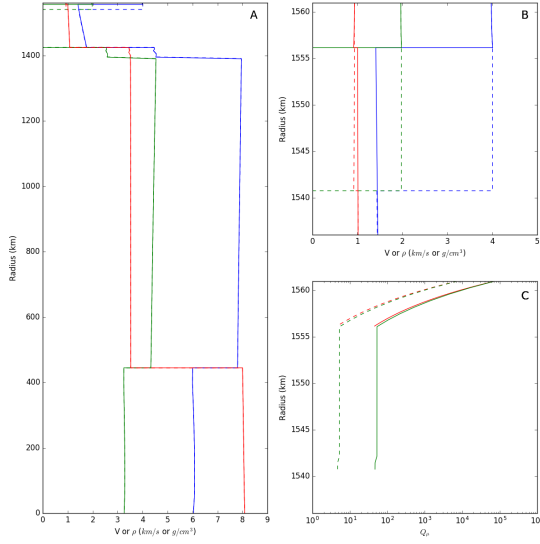


Figure 2. (A) V_P (blue), V_S (green), and density (blue) for the 5 km thick ice shell model (solid) and 20 km thick ice shell model (dashed). (B) Same as (A), but zoomed in to show ice shell and upper ocean structure. (C) Q_μ values for the ice shells for the 5 km thick ice shell (red) and 20 km thick shell (green) for the high (solid) and low Q (dashed) models.

in which $B_a = 0.56$ is a normalization factor, ω is the seismic frequency, exponent $\gamma = 0.2$ is the frequency dependence of attenuation, and R is the ideal gas constant. H , the activation enthalpy, scales with the melting temperature T_m and with the anisotropy coefficient g_a , and the values of g_a chosen for various ices are described in Vance *et al.* [2017b]. The bulk quality factor, Q_κ , is neglected. This relationship predicts very high Q values, and therefore very little attenuation, within the ice shell (fig. 2C). However, attenuation in ice at very low temperatures is not very well constrained. Although studies of glacier ice suggest near-surface layers can have very low Q [Gusmeroli *et al.*, 2010], high Q values are reached at low temperatures. Fractured ice may also be more attenuating than simple melting temperature scaled solid ice estimates, and partial but incomplete saturation with fluids can lower Q even further [Peters *et al.*, 2012]. For these reasons, we choose to use two different Q structures: one predicted by equation 5, and one with Q arbitrarily reduced by a factor of 10. Combining the 2 different ice shell thicknesses and 2 different Q structures explored, we have 4 structure models to explore in this study. Combined with the 5 seismicity models discussed in section 2, we have 20 different noise simulations to create.

4 Noise estimates

With the catalogs based on assumed Gutenberg-Richter relationships and the thermodynamically self-consistent models in place, we have the ingredients to create synthetic noise records representing the expected background noise due to cracking events in the ice. In order for these to be useful, we need to be able to rapidly calculate waveforms for arbitrary source locations up to frequencies near 1 Hz for thousands to tens of thousands of events. Fortunately, the python-based Instaseis program [van Driel *et al.*, 2015] is well-suited for problems of this type. Instaseis makes use of full waveform databases computed with the axisymmetric spectral element code AxiSEM [Nissen-Meyer *et al.*, 2014]. These databases are

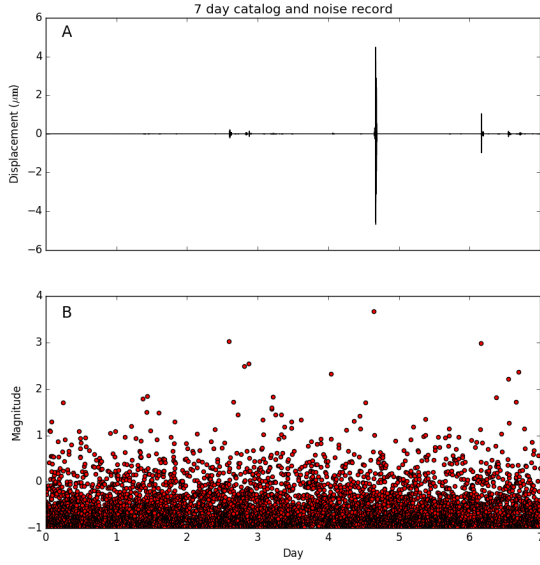


Figure 3. Sample noise record (A) plotted for a 1 week realization of the “preferred” seismicity model (B) in the 5 km ice shell model with high Q .

computed for 2 sources (one vertical force and one horizontal) located at the surface at the north pole in a 1D spherically symmetric planetary model, which can then be rapidly interpolated to arbitrary source and receiver geometries using the principle of reciprocity. This allows for rapid seismogram calculation, from milliseconds to seconds on a desktop processor depending on length and frequency content of the waveform database, although the initial waveform database is a larger computational investment. AxiSEM is readily able to handle arbitrary planetary models, as demonstrated by the exploration of ocean world seismology by *Stähler et al.* [2017].

The catalogs of section 2, which initially were only calculated to give a time-series of quake occurrence, need to be completed by specifying all the relevant source characteristics. For this exercise, we assumed a polar location for our station and a homogenous distribution of epicenters on the surface of the planet. Depth was randomly assigned between the surface and 2 km depth, a commonly assumed depth of the brittle-ductile transition [*Pappalardo et al.*, 1999]. Strike, rake, and dip were also randomly assigned. Clearly, the real seismicity on Europa will likely be influenced by the tidal stress pattern, causing variations in seismicity rate in both time and space, but a homogenous distribution was chosen as an initial baseline estimation of the kind of seismic activity we could expect for a landed seismometer on the surface of Europa. Once these source characteristics are defined for the catalog, we generate noise records using Instaseis with all events calculated using AxiSEM databases with 1 hour databases calculated to a dominant frequency of 1 Hz. Figure 3 displays a typical seismic trace realized for a 1 week catalog based on the “preferred” seismicity model. Note that the record is dominated by a handful of larger events, which is typical for any record calculated with a Gutenberg-Richter relationship with a b value of 1. Between these larger events, however, a background level of seismic energy develops from the large numbers of smaller events (e.g. figures 1B and 3B).

In order to determine reasonable spectral characteristics of the average power of the ambient noise from this record, we need to be careful to not simply estimate power spectral density of the whole record. This will be dominated by the sporadic large events, and not

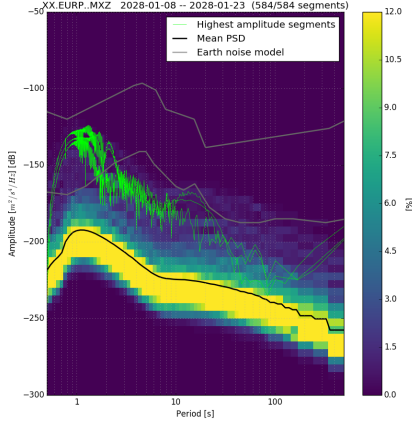


Figure 4. An example probabilistic power spectral density for the 5 km thick ice shell high Q model with the preferred seismicity model. Background colors are the probability density function of ground acceleration power using 584 partially overlapping 1 hour segments covering 2 weeks of simulated noise records. The solid black line represents the mean PSD, while the thin green lines represent the PSDs for the highest three 1 hour segments. Note that the peak amplitudes are 40–50 dB above the mean background noise. Grey lines represent the low and high noise models for background noise observed at Earth stations [Peterson, 1993].

represent the power in the noise between these events, which is what the sensor will record the majority of the time. To account for this, we use a probabilistic approach to determining the power spectral density (PSD) that is commonly used when assessing noise levels recorded by seismic stations on Earth [McNamara and Buland, 2004]. This is implemented by the PPSD tool in the signal processing toolkit of ObsPy [Krischer et al., 2015], which is a seismic package for Python. In this approach, the record is divided into a series of overlapping 1 hour segments, and a PSD is determined for each segment. These are then stacked in order to obtain a probability density function of the noise (fig. 4).

5 Results

For each combination of our 4 structural models and 5 seismicity models, we calculated a probabilistic PSD estimate of the ground acceleration noise power analogous to fig. 4. In order to facilitate plotting multiple estimates on a single axis, we instead plot only the mean value (i.e. the black line in fig. 4) for all seismicity models on the same axis for each structural model (fig. 5). To give context to these noise estimates, we also plot the low and high noise models for the Earth [Peterson, 1993], as well as self-noise models for several seismic instruments, ranging from an industry standard for high quality broadband instruments [the STS2 with the dark red dashed line, Ringler and Hutt, 2010] to a readily available low cost high frequency geophone [dashed black line, Rodgers, 1994]. In between are the noise estimates for a Trillium Compact instrument [Ringler and Hutt, 2010], which is a common instrument used in Earth applications, and the SP instrument built for the InSight mission to Mars, due to launch in 2018 [Pike et al., 2016]. These two instruments have a similar noise floor between the top-of-the-line broadband instruments and the high-frequency geophones.

For the overall noise level, both the 5 km and 20 km thick ice shell models produce similar amplitudes at the highest frequencies we explored near 1 Hz (fig. 5). The thinner ice shell models have higher amplitudes at lower frequencies, with a difference of 10–20 dB near

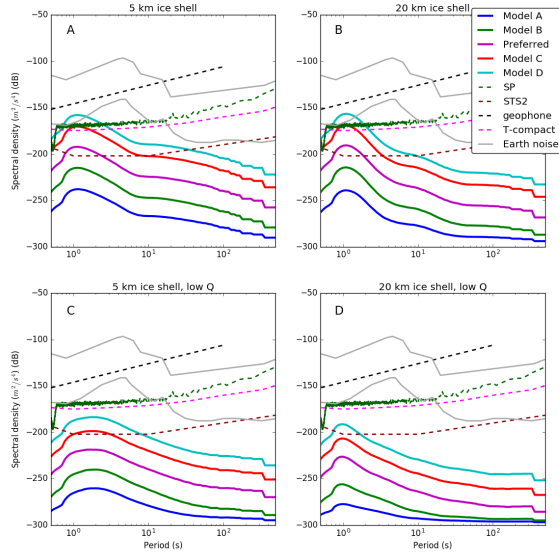


Figure 5. Summary noise figures plotting mean PSD estimates for noise models in 5 km thick (A and C) and 20 km thick ice shell models (B and D) assuming high Q (A and B) or low Q in the ice shell (C and D). For each model, the mean PSD estimate is plotted for the five seismicity models as solid lines. Low and high noise models for the Earth are plotted in grey [Peterson, 1993]. For comparison, self-noise curves for broadband STS2 and Trillium Compact Earth instruments [Ringler and Hutt, 2010], the SP instrument which will be launched with the InSight mission [Pike et al., 2016] and a typical high frequency geophone [Rodgers, 1994].

periods of 10 s, depending on whether we are comparing the low or high Q models. This is consistent with the signal of large amplitude lower frequency flexural waves predicted for thinner ice shells [Panning *et al.*, 2006]. As expected, the lower Q models also predict lower amplitude noise models, with the factor of 10 difference in Q here leading to approximately 20 dB lower power signal near 1 Hz in the low Q models compared to the high Q models of the same thickness. The range of seismicity models explored here, however, are the biggest source of uncertainty. The difference in signal power between the high seismicity model D and low seismicity model A leads to a ~ 80 dB offset of our final noise power estimates.

Compared with the instrument noise curves, we can see that a relatively low sensitivity geophone is unlikely to record the ambient noise due to tidal cracking, regardless of the model chosen or the seismicity level. More sensitive instruments like the InSight SP may be able to record this kind of ambient noise for higher overall seismicity levels, at least near 1 Hz, and a very sensitive instrument may be able to record over a broader frequency range out to 10 s period for the highest seismicity levels.

The peak recorded signals, though, representing the largest events during the span of 2 to 3 weeks, rise 30–50 dB above the mean noise level (fig. 4), and are thus likely recordable between 1 Hz and 10 s period with an instrument similar in quality to the SP instrument or Trillium compact. This separation of 30–50 dB is actually a conservative estimate, as it is based only on 1 hour calculations for the PSD. A window chosen to specifically highlight the event would return a slightly higher power estimate. In fact, specific phases of interest like body waves which may record ice shell and ocean reflections [e.g. Lee *et al.*, 2003], or the Crary phase which is sensitive to ice shell thickness [e.g. Vance *et al.*, 2017a], or the surface waves, including flexural waves [e.g. Panning *et al.*, 2006] rise above both instrument noise curves and background noise levels (fig. 6). The traces shown in figure 6 rise above the background noise even though they include an approximation of the effects of moderate scattering (see section 6.3 for details about how this is implemented). These are calculated for a moment magnitude (M_W) 3.1 event 90° from the lander. This is a reasonable estimate for the largest event recorded in a few weeks given our preferred seismicity model (fig. 1). Even these high amplitude arrivals, though, only just begin to approach the self-noise floor of the high frequency geophone. This estimate, however, is based on a relatively distant event, which is reasonable if we assume a homogenous, random distribution of events with a landing site that is not chosen to maximize probability of recording an event. In this case the vast majority of events recorded will take place between 45° and 135° from the lander based simply on surface area of a sphere. If a landing site on Europa (or similarly for Enceladus or Titan) were chosen to be close to areas of observed activity (such as observed plumes or modeled maximal tidal stresses), it may be reasonable to expect larger events closer to the lander, and a less sensitive instrument may be sufficient. Further modeling of expected activity would then be essential.

6 Discussion

6.1 Autocorrelation of ambient noise

While our initial results suggest ambient noise due to cracking events alone may be hard to reliably record, there will likely be other noise sources such as ocean noise (see section 6.2). Regardless of the source of noise, we may be able to use reliable recordings of background noise (i.e. background noise above the instrument self-noise) to extract useful information about structure, even in the absence of identifiable larger ice tectonic events. Claerbout [1968] suggested that autocorrelation of ambient noise should produce the equivalent reflection response as if you had a source co-located with the receiver, and this approach has been applied numerous times since then using either earthquake coda [e.g. Wang *et al.*, 2015; Huang *et al.*, 2015] or ambient seismic noise [e.g. Tibuleac and von Seggern, 2012; Kennett, 2015; Saygin *et al.*, 2017]. Zhan *et al.* [2013] explored the use of noise autocorrelation in a potentially analogous setting for a deployment of broadband seismometers at 24

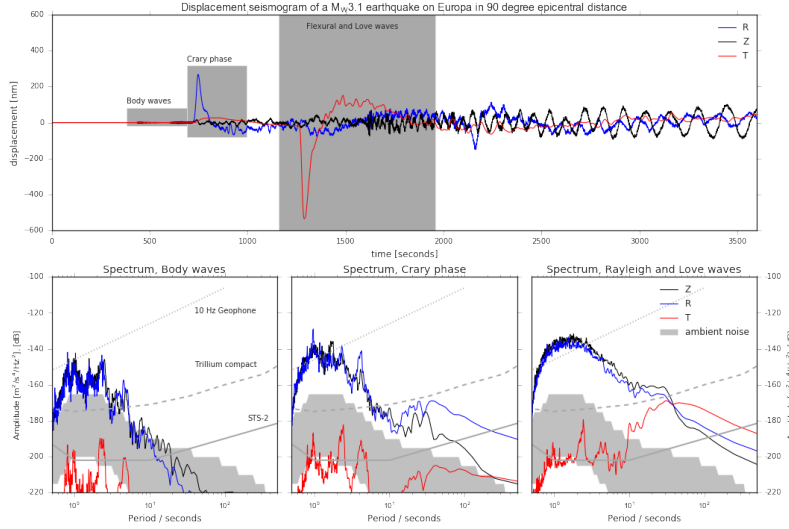


Figure 6. Three component seismogram (vertical component black, horizontal component along the great circle between source and receiver in blue, and perpendicular to the path in red) for a $M_W 3.1$ event at a depth of 2 km at a 90° epicentral distance from the station in the 5 km ice shell high Q model (top). Approximate scattering in the ice shell is included (see section 6.3 for details). Bottom row shows spectra for the three grey windows for the three components. Grey field in lower panels spans the range between the mean PSD for the preferred model through model D.

different sites on the Amery Ice Shelf, Antarctica. While for most sites, the incoherent noise (e.g. the mechanical and electrical noise of the station installation) exceeded the coherent noise, the authors were able to identify resonances in spectral ratios of the three component data of one station which were modeled as resonances due to P waves in the water layer between the ice and seafloor.

In order to test the feasibility of such an approach with a noise source like the one modeled in this study, we calculated autocorrelation functions, following the approach of *Huang et al.* [2015]. For this test we used the vertical component of a 1-week noise record in the 20-km ice shell model with low Q . The resulting response (fig. 7, top line) shows a clear arrival near 175 seconds, which represents the reflection from the ocean floor. There also appear to be arrivals that correlate with the first and second multiples of that reflection, which are clearly shown in the trace calculated using Instaseis for a co-located source and receiver (fig. 7, bottom line), although the multiples cannot be easily distinguished from the background oscillations in the autocorrelation function. Details of the autocorrelation function depend strongly on choices of filtering and autocorrelation window length, and while this particular model appears to show the multiples, we can generally only robustly see the first reflection using other noise records and Europa structure models. Even this first reflection, however, would allow for rapid determination of total ocean depth, even in the absence of any other tectonic events.

Identification of such signals requires careful processing and filtering of the data, so it may be possible to find other signals in the horizontal components or using other processing that may also constrain other values of interest, like the ice shell thickness. Resonances may also be easier to detect with spectral ratios, as shown by data from the Amery Ice Shelf [*Zhan et al.*, 2013]. In this test, though, we did not include any estimate of the observing instrument self-noise. As illustrated by *Zhan et al.* [2013], however, coherent noise (due to propagating waves) needs to exceed incoherent noise across the filtered frequency band in

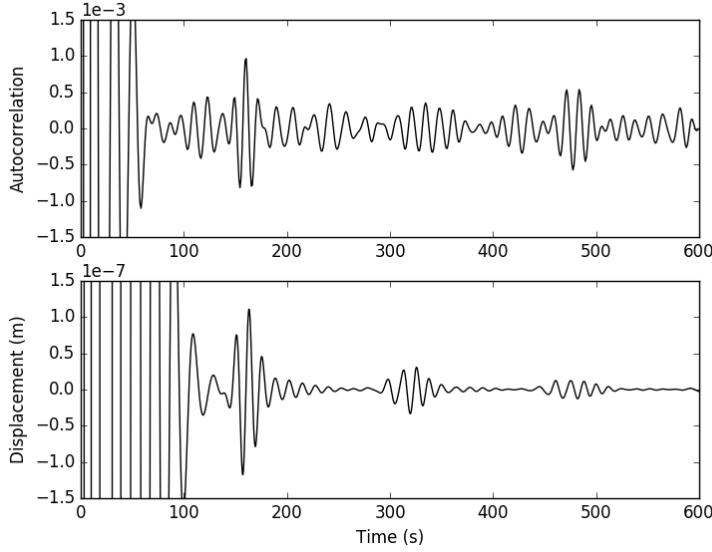


Figure 7. Autocorrelation function (top) calculated from one week of simulated noise using the Model C seismicity and the Europa model with 20 km thick ice shell and low Q compared to the zero offset displacement trace calculated using a single vertical force of 10^{10} N (bottom). Both traces are filtered between 0.05 and 0.1 Hz.

order to obtain reliable autocorrelation information. That will clearly be very challenging or impossible in the frequency band shown in figure 7 based on the mean PSD estimates discussed in this study, unless activity level is at or above the highest levels explored here and a very sensitive instrument, such as the STS2 or the VBB instrument from the InSight mission [Lognonné and Pike, 2015], is used. Realistically, such observations are likely only going to be possible if it will be possible to select data from high noise periods that may exist due to temporal variability due to diurnal tidal variations or other processes.

6.2 Ocean noise

On the Earth, ambient noise at most stations is dominated by microseisms, which originate in the ocean due to pressure variations at the ocean floor related to wave interactions [Longuet-Higgins, 1950]. While a subsurface ocean will not have the wind-driven gravity waves observed in the Earth’s ocean, tidal deformation will generate motions in the ocean. A study of the turbulent flow produced in the ocean suggests that there may be significant radial flow velocities approaching 2.5 m/s immediately below the ice shell [Soderlund *et al.*, 2014]. We convert these velocities to dynamic pressures acting on the base of the ice shell using the relationship $P = \frac{1}{2}\rho U^2$, where P is pressure, ρ is fluid density, and U is radial flow velocity. Associated pressure variations are a few kPa, which is comparable to pressure variations at the floor of Earth’s ocean.

The simulation of Soderlund *et al.* [2014] only modeled motions with periods longer than ~ 1000 s, so the excitation occurs at significantly longer periods than we have focused on with the ice tectonic sources. To model this in the range of frequencies discussed in this study, we create a random radial velocity model (fig. 8), which we convert to dynamic pressure at the base of the ice shell, as an input source to Instaseis. This allows us to generate noise time series comparable to those we calculated for the ice tectonic sources. We generate a random velocity field that is correlated in both space and time as defined by a von

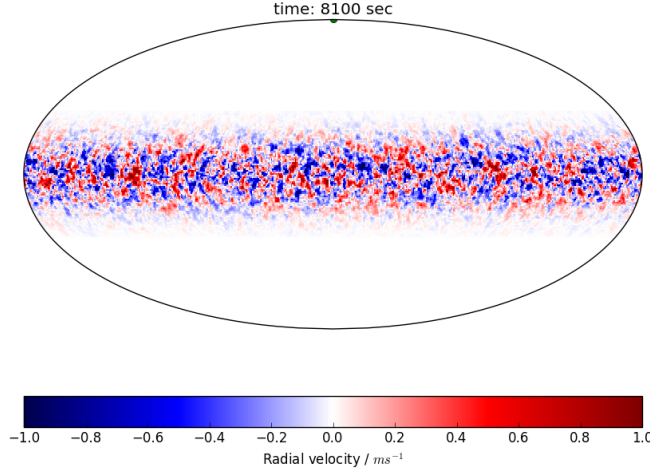


Figure 8. An example random radial ocean velocity field time slice generated as described in the text with parameters chosen to match the general characteristics of the model of *Soderlund et al.* [2014].

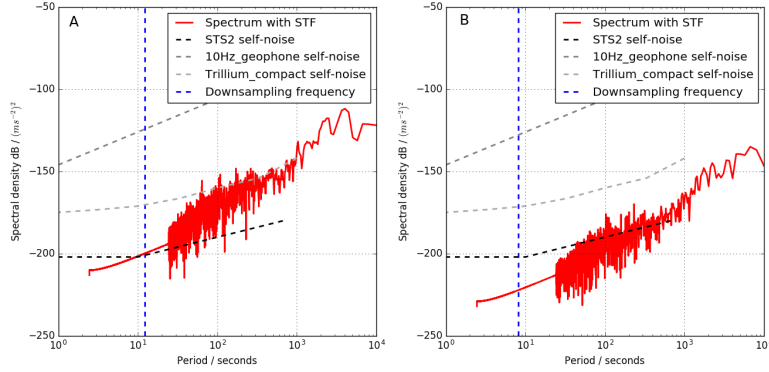


Figure 9. Calculated noise spectra from modeled ocean pressure variations at the base of the ice shell in the 20 km model with high Q at the equator (A) and north pole (B) compared with instrument self-noise curves.

Karman autocorrelation function, as has long been used in defining randomly perturbed seismic media [e.g. *Sato*, 1982], with correlation lengths of 50 km in latitudinal and longitudinal directions and 1000 s in time. The structure is confined to within 20° of the equator, compatible with the larger amplitudes observed near the equator in the model of *Soderlund et al.* [2014], as seen in the example time slice shown in figure 8. The amplitudes of velocities are set to vary on the scale of ± 1 m/s in order to be comparable with the model of *Soderlund et al.* [2014].

The resulting seismic noise spectra produced by such a model are shown for the 20 km thick model with high Q . The noise amplitude depends on the latitude of observation, with significantly larger amplitudes at the equator than the poles (fig. 9). The equatorial signal is comparable with the noise floor of the SP or Trillium compact instruments. In each case, the spectrum drops off at higher frequencies, and this drop-off is a function of the drop-off of the spectrum of the von Karman source-time functions. If we used another method to extrapolate to higher frequencies, it is possible that this slope could change, but this indicates that ocean

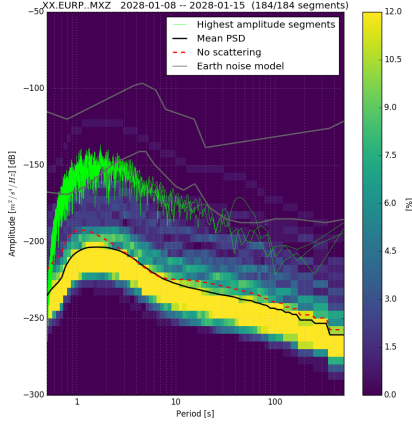


Figure 10. Same as figure 4, but using a model including heterogeneity to simulate moderate scattering within the great-circle path between source and receiver. The mean PSD for the case with no scattering is plotted as a red dashed line.

turbulence may create enough pressure signal to be observable with potential planetary seismic instruments.

As discussed by *Zhu et al.* [2017], however, the values of the ocean thermal diffusivity and vertical temperature gradient utilized by *Soderlund et al.* [2014] may be unreasonably large. If this is the case, turbulent flow velocities could be considerably lower than estimated here. In fact, they may be low enough that global variations in ice shell thickness produce a stratified layer of lower salinity water in the region of ice melting [*Zhu et al.*, 2017]. Such a stratification would act to further dampen radial flow velocities at the base of the ice shell, decreasing the estimated ocean noise.

6.3 Effects of scattering

All the modeling done to this point has assumed simple 1D models of structure for Europa. Real data, however, are affected by small-scale structure which scatters seismic energy from the simple geometric paths predicted in a layered 1D model. For example, our only other high-quality planetary dataset including clear tectonic events, the Apollo catalog of lunar seismic data, is dominated by scattering originating in a regolith layer that is highly fractured, but with very little intrinsic attenuation [e.g. *Goins et al.*, 1981]. Such scattering can greatly change the character of a seismic record, reducing the amplitude of geometric phase arrivals as energy is scattered from the geometric path, while simultaneously producing extended codas (which on the Moon can continue for an hour or longer) representing energy that propagated longer distances due to off-path scattering. In the absence of attenuation, such effects should not cause significant changes, however, to the frequency characteristics of noise, as the scattering simply shifts energy of a given frequency in time from geometric arrivals to extended codas. Spectra estimated over sufficiently long durations should show similar characteristics in this case. In the presence of attenuation, though, the longer scattered paths will allow for more energy loss due to intrinsic attenuation.

Modeling strong 3D scattering like the Moon's requires either very finely sampled (and thus computationally intensive) numerical wave propagation or clever statistical techniques like a seismic phonon method [e.g. *Blanchette-Guertin et al.*, 2015]. Such approaches can include multiply scattered energy from anywhere in the planet. This modeling, however, is beyond the scope of this initial study of the Europa noise environment. We can model simpler

scattering due to relatively long-wavelength structure within the great-circle path between source and receiver using the AxiSEM/Instaseis approach of this study.

The scattering model used here is discussed more thoroughly in *Stähler et al.* [2017]. We implement a von Karman random medium with a correlation length of 5 km and velocity variations of 10%. As before, we calculate an hour-long waveform database using AxiSEM and then use Instaseis in combination with our seismicity catalogs to estimate a continuous noise record which is used to estimate a PSD for the noise (fig. 10). We show the results for a scattering model superimposed over the high Q model with a 5 km ice shell. The general character of the noise is similar, however there is a significant reduction in the mean PSD amplitude for periods shorter than a few seconds. Some of this effect may be partially due to longer scattering paths pushing energy outside of the hour-long waveform records used for our noise calculation, but it is likely that this is mostly due to greater loss of energy to attenuation due to longer scattered path lengths at higher frequencies. Large events still show a similar offset by 30–50 dB as seen in the unscattered records, but the peak energy is shifted to slightly lower frequency compared to the unscattered case.

6.4 Effects of regolith

On an airless body, a surface regolith that is highly fractured with void-filled cracks formed by impact gardening or tidal tectonic fracturing is likely, although the depth of such a layer on Europa is difficult to estimate. Coherent backscatter of Earth-based radar measurements suggest a high porosity (25–75%) layer extending to depths of up to a few meters at most [*Black et al.*, 2001], which is consistent with scatterers that are either filled with void or contrasting ice. This could represent an impact gardened regolith, which can be modeled based on craters to extend up to a few meters deep [e.g. *Moore et al.*, 2008]. *Eluskiewicz* [2004] proposed a regolith layer could reach a thickness in excess of 1 km based on estimates of compaction timescales as a function of depth. A more recent response to that work has been updated to more accurately model development of regolith due to tidal fracturing (rather than impact gardening) along with modeled temperature profiles to determine where ice creep rates would be sufficient to close any open pores. A large range of models was possible with depths of such a regolith varying between 0.5 and 3 km, with porosities varying between 1 and 22% [*Aglyamov et al.*, 2017]. Whatever the thickness, such a layer would likely introduce more intense 3D scattering than that modeled in section 6.3. Modeling such a layer is beyond the scope of the current study as it will require computationally intensive 3D numerical wave propagation codes or explorations using stochastic methods based on radiative transfer theory [e.g. *Gillet et al.*, 2016] or the seismic phonon method [e.g. *Blanchette-Guertin et al.*, 2015], but we can consider qualitatively how such a layer may affect seismic data recovered from a landed Europa mission.

Such a layer will likely act to reduce the amplitude of any Crary waves observed in the data, since the Crary waveguide relies on homogenous properties of the ice shell giving rise to perfect reflections at the surface and base of the ice shell for SV waves with a horizontal slowness equal to that of a P wave propagating in the ice shell [*Crary*, 1954; *Vance et al.*, 2017a; *Stähler et al.*, 2017]. However, the scattering and coda such a layer produces could be used to increase other kinds of science return from seismic data. For example, the scattered seismic energy either in ambient noise or coda of phase arrivals could be used to extract high frequency Rayleigh wave ellipticity information (greater than 1 Hz), which has been proposed for use in constraining near-surface structure on Mars using data from the upcoming InSight mission [*Knapmeyer-Endrun et al.*, 2016]. Further investigation of possible effects of regolith scattering will likely be essential in order to understand any returned seismic data from Europa.

6.5 Spatiotemporal variation

For simplicity, we have assumed that seismicity follows a statistical Gutenberg-Richter relationship that is stationary in both time and space. The tidal stresses on Europa, though, vary as a function of time and space during each orbital cycle around Jupiter [e.g. *Greenberg et al.*, 1998]. This implies that the noise estimated in this study can only be considered a mean value, and the actual levels will vary depending on the choice of landing site and within each ~ 85 hour tidal cycle. Consideration of this tidal variation as well as likely spatial variation in ocean noise generation as discussed in section 6.2 will be critical in landing site selection to maximize seismic data return.

6.6 Instrument requirements

Following *Lee et al.* [2003], the recently released report of the Europa Lander Science Definition Team [*Hand et al.*, 2017] argued for a noise floor of -35 dB with respect to a velocity of $1 \mu\text{m/s}$ in order to establish a preliminary instrument requirement. If we treat this floor as flat in velocity, and convert to the acceleration power spectral density relative to 1 m/s^2 used in this study, this would correspond to approximately -175 dB at 1 Hz and -185 dB at a period of 10 s, which is comparable to the mean PSD values for the “model C” seismicity model in the high Q Europa models. This suggests our approach is broadly consistent with previous noise estimates, and further suggests that both estimates of the noise floor indicate that a high frequency geophone is likely not sufficient to meet science requirements for a landed Europa mission, without relying on future modeling and observations to allow us to specifically pick a landing site near expected activity. Meanwhile an instrument with sensitivity similar to the Trillium Compact or the InSight SP instrument will more likely meet science requirements based on the homogenous modeling developed here. Specifically, it should be able to reliably record important phase signals from larger events (i.e. signal), and may be able to record the background ambient noise if the actual seismic activity is in the higher range of our estimates, or in time periods of higher activity in the tidal cycle.

This study primarily focused on the noise recorded on the vertical component, which often has the lowest noise due to local site effects in Earth settings, but future work will also need to focus on noise and signals from the horizontal components in order to more fully evaluate the relative utility of sending a 3 component instrument or simply a 1-axis vertical instrument. This will also help inform mission design on requirements of alignment of sensors, such as the need for a leveling system or control of horizontal component azimuthal orientation. Polarization information is essential for determination of back azimuth in single station location techniques [e.g. *Panning et al.*, 2015], and access to wave types with horizontal polarization provides important constraints on relevant parameters [further discussion in *Stähler et al.*, 2017], and so a 3 component instrument should have significant advantages. Further work, though, will be required to look not just at ambient noise sources, but also details of installation and lander noise.

7 Conclusions

In order to estimate the likely seismic noise levels for an instrument on Europa’s surface, we explore a range of seismicity models that follow a Gutenberg-Richter relationship. The seismic activity level in such models depend on the cumulative seismic moment release and maximum event size. Given a range of reasonable values for these parameters scaled from observed activity levels on the Moon, we generate catalogs, and then use them to generate models of seismic noise using numerical wave propagation codes through thermodynamically consistent models of Europa’s interior structure.

Given this range of models, we show that most reasonable models show background noise levels well below the sensitivity of a high frequency geophone, but potentially measurable by more sensitive instruments particularly for the higher seismicity models. The ampli-

tudes of the largest events observable in a given period of a few weeks are likely observable by more sensitive broadband instruments analogous to a Trillium Compact or the InSight SP instrument.

We demonstrate the potential of auto-correlation of such noise records to determine the ocean depth. We also explore the possible amplitude of noise generated by turbulent flow in the subsurface ocean due to tidal motions. Such a noise source may be observable with reasonable planetary seismic instruments at longer periods.

Acknowledgments

The authors acknowledge computational support in the project pr63qo "3D wave propagation and rupture: forward and inverse problem" at *Leibniz-Rechenzentrum* Garching. SCS was supported by grant SI1538/4-1 of Deutsche Forschungsgemeinschaft *DFG*. This work was partially supported by strategic research and technology funds from the Jet Propulsion Laboratory, Caltech, and by the Icy Worlds node of NASA's Astrobiology Institute (13-13NAI7_2-0024). Noise records and seismic catalogs are available via GitHub at <http://github.com/mpanning/EuropaNoise>. Waveform databases are maintained by SCS and will be made available upon request. All rights reserved prior to publication.

References

- Aglyamov, Y., D. M. Schroeder, and S. D. Vance (2017), Bright prospects for radar detection of Europa's ocean, *Icarus*, *281*, 334–337, doi:10.1016/j.icarus.2016.08.014.
- Beuthe, M. (2015), Tides on Europa: The membrane paradigm, *Icarus*, *248*, 109–134, doi:10.1016/j.icarus.2014.10.027.
- Bills, B. G., F. Nimmo, O. Karatekin, T. Van Hoolst, N. Rambaux, B. Levrard, and J. Laskar (2009), Rotational dynamics of Europa, in *Europa*, edited by R. T. Pappalardo, W. McKinnon, and K. Khurana, pp. 119–136, Univ. Arizona Press, Tucson.
- Black, G. J., D. B. Campbell, and P. D. Nicholson (2001), Icy Galilean satellites: Modeling radar reflectivities as a coherent backscatter effect, *Icarus*, *151*, 167–180, doi:10.1006/icar.2001.6616.
- Blanchette-Guertin, J.-F., C. L. Johnson, and J. F. Lawrence (2015), Modeling seismic energy propagation in highly scattering environments, *J. Geophys. Res.*, *120*(3), 515–537, doi:10.1002/2014JE004654.
- Camarano, F., V. Lekić, M. Manga, M. P. Panning, and B. A. Romanowicz (2006), Long-period seismology on Europa: 1. Physically consistent interior models, *J. Geophys. Res.*, *111*, E12,009, doi:10.1029/2006JE002710.
- Campillo, M., and A. Paul (2003), Long-range correlations in the diffuse seismic coda, *Science*, *229*, 547–549.
- Chyba, C. F., S. J. Ostro, and B. C. Edwards (1998), Radar detectability of a subsurface ocean on Europa, *Icarus*, *134*, 292–302.
- Claerbout, J. F. (1968), Synthesis of a layered medium from its acoustic transmission response, *Geophysics*, *33*, 264–269.
- Crary, A. P. (1954), Seismic studies on Fletcher's Ice Island, T-3, *EOS Trans. AGU*, *35*(2), 293–300, doi:10.1029/TR035i002p00293.
- Eluskiewicz, J. (2004), Dim prospects for radar detection of Europa's ocean, *Icarus*, *170*, 234–236, doi:10.1016/j.icarus.2004.02.011.
- Frohlich, C., and S. D. Davis (1993), Teleseismic *b* values; Or, much ado about 1.0, *J. Geophys. Res.*, *98*(B1), 631–644, doi:10.1029/92JB01891.
- Gillet, K., L. Margerin, M. Calvet, and M. Monnerau (2016), Scattering attenuation profile of the Moon: Implications for shallow moonquakes and the structure of the megaregolith, *Phys. Earth Planet. Int.*, *262*, 28–40, doi:10.1016/j.pepi.2016.11.001.
- Goins, N. R., A. M. Dainty, and M. N. Toksöz (1981), Lunar seismology: the internal structure of the Moon, *J. Geophys. Res.*, *86*(B6), 5061–5074, doi:10.1029/JB086iB06p05061.

- Golombek, M., W. Banerdt, K. Tanaka, and D. Tralli (1992), A prediction of Mars seismicity from surface faulting, *Science*, 258, 979–981.
- Grasset, O., M. K. Dougherty, A. Coustenis, E. J. Bunce, C. Erd, D. Titov, M. Blanc, A. Coates, P. Drossart, L. N. Fletcher, H. Hussmann, R. Jaumann, N. Krupp, and J.-P. Lebreton (2013), JUPiter ICy moons Explorer (JUICE): An ESA mission to orbit Ganymede and to characterise the Jupiter system, *Plan. & Space Sci.*, 78, 1–21, doi:10.1016/j.pss.2012.12.002.
- Greenberg, R., P. Geissler, G. Hoppa, B. R. Tufts, D. D. Durda, R. Pappalardo, J. W. Head, R. Greeley, R. Sullivan, and M. H. Carr (1998), Tectonic processes on Europa: Tidal stresses, mechanical response, and visible features, *Icarus*, 135(1), 64–78, doi:10.1006/icar.1998.5986.
- Gusmeroli, A., R. A. Clark, T. Murray, A. D. Booth, B. Kulesa, and B. E. Barrett (2010), Seismic wave attenuation in the uppermost glacier ice of Storglaciären, Sweden, *J. Glac.*, 56(196), 249–256, doi:10.3189/002214310791968485.
- Gutenberg, B., and C. F. Richter (1944), Frequency of earthquakes in California, *Bull. Seism. Soc. Am.*, 34, 185–188.
- Hand, K. P., A. E. Murray, J. B. Garvin, W. B. Brinckerhoff, B. C. Christner, K. S. Edgett, B. L. Ehlmann, C. R. German, A. G. Hayes, T. M. Hoehler, S. M. Horst, J. I. Lunine, K. H. Nealson, C. Paranicas, B. E. Schmidt, D. E. Smith, A. R. Rhoden, M. J. Russell, A. S. Templeton, P. A. Willis, R. A. Yingst, C. B. Phillips, M. L. Cable, K. L. Craft, A. E. Hofmann, T. A. Nordheim, R. P. Pappalardo, and the Project Engineering Team (2017), Report of the Europa Lander Science Definition Team, *Tech. Rep. JPL D-97667*, NASA.
- Hoppa, G. V., B. R. Tufts, R. Greenberg, and P. E. Geissler (1999), Formation of cycloidal features on Europa, *Science*, 285, 1899–1902.
- Huang, H.-H., F.-C. Lin, V. C. Tsai, and K. D. Koper (2015), High-resolution probing of inner core structure with seismic interferometry, *Geophys. Res. Lett.*, 42, 10,622–10,630, doi:10.1002/2015GL066390.
- Hurford, T. A., A. R. Sarid, and R. Greenberg (2007), Cycloidal cracks on Europa: Improved modeling and non-synchronous rotation implications, *Icarus*, 186, 218–233, doi:10.1016/j.icarus.2006.08.026.
- Hussmann, H., and T. Spohn (2004), Thermal-orbital evolution of Io and Europa, *Icarus*, 171(2), 391–410, doi:10.1016/j.icarus.2004.05.020.
- Kanamori, H. (1977), The energy release in great earthquakes, *J. Geophys. Res.*, 82, 2981–2987, doi:10.1029/JB082i020p02981.
- Kennett, B. L. N. (2015), Lithosphere-asthenosphere P-wave reflectivity across Australia, *Earth Planet. Sci. Lett.*, 431, 225–235, doi:10.1016/j.epsl.2015.09.039.
- Kivelson, M. G., K. K. Khurana, C. T. Russell, M. Volwerk, R. J. Walker, and C. Zimmer (2000), Galileo magnetometer measurements: A stronger case for a subsurface ocean at Europa, *Science*, 289(5483), 1340–1343, doi:10.1126/science.289.5483.1340.
- Knapmeyer-Endrun, B., M. P. Golombek, and M. Ohnberger (2016), Rayleigh wave ellipticity modeling and inversion for shallow structure at the proposed InSight landing site in Elysium Planitia, Mars, *Space Sci. Rev.*, doi:10.1007/s11214-016-0300-1.
- Kohlhase, C., and P. Penzo (1977), Voyager mission description, *Space Sci. Rev.*, 21(2), 77–101, doi:10.1007/BF00200846.
- Kovach, R. L., and C. F. Chyba (2001), Seismic detectability of a subsurface ocean on Europa, *Icarus*, 150, 279–287, doi:10.1006/icar.2000.6577.
- Krischer, L., T. Megies, R. Barsch, M. Beyreuther, T. Lecocq, C. Caudron, and J. Wasserman (2015), ObsPy: a bridge for seismology into the scientific Python ecosystem, *Comp. Sci. Disc.*, 8(1), 014,003, doi:10.1088/1749-4699/8/1/014003.
- Lammlein, D., G. Latham, J. Dorman, Y. Nakamura, and M. Ewing (1974), Lunar seismicity, structure and tectonics, *Rev. Geophys. Space Phys.*, 12, 1–21.
- Lee, S., M. Zanolin, A. M. Thode, R. T. Pappalardo, and N. C. Makris (2003), Probing Europa's interior with natural sound sources, *Icarus*, 165, 144–167, doi:10.1016/S0019-1035(03)00150-7.

- Lee, S., R. T. Pappalardo, and N. C. Makris (2005), Mechanics of tidally driven fractures in Europa's ice shell, *Icarus*, *177*, 367–379, doi:10.1016/j.icarus.2005.07.003.
- Lognonné, P., and W. T. Pike (2015), Planetary seismometry, in *Extraterrestrial Seismology*, edited by V. C. H. Tong and R. Garcia, chap. 3, pp. 36–48, Cambridge Univ. Press, Cambridge, U.K., doi:10.1017/CBO9781107300668.006.
- Longuet-Higgins, M. S. (1950), A theory of the origin of microseisms, *Phil. Trans. R. Soc. Lond. A*, *243*(857), 1–35.
- McNamara, D. E., and R. P. Buland (2004), Ambient noise levels in the continental United States, *Bull. Seism. Soc. Am.*, *94*(4), 1517–1527.
- Moore, J. M., G. Black, B. Buratti, C. B. Phillips, J. Spencer, and R. Sullivan (2008), Surface properties, regolith, and landscape degradation, in *Europa*, edited by R. T. Pappalardo, W. B. McKinnon, and K. Khurana, pp. 329–349, Univ. Arizona Press.
- Nimmo, F., and P. Schenk (2006), Normal faulting on Europa: implications for ice shell properties, *J. Struct. Geol.*, *28*, 2194–2203, doi:10.1016/j.jsg.2005.08.009.
- Nissen-Meyer, T., M. van Driel, S. C. Stähler, K. Hosseini, S. Hempel, L. Auer, A. Colombi, and A. Fournier (2014), AxiSEM: broadband 3-D seismic wavefields in axisymmetric media, *Solid Earth*, *5*(1), 425–445.
- Oberst, J. (1987), Unusually high stress drops associated with shallow moonquakes, *J. Geophys. Res.*, *92*(B2), 1397–1405, doi:10.1029/JB092iB02p01397.
- Panning, M. P., V. Lekić, M. Manga, F. Cammarano, and B. A. Romanowicz (2006), Long-period seismology on Europa: 2. Predicted seismic response, *J. Geophys. Res.*, *111*, E12,008, doi:10.1029/2006JE002712.
- Panning, M. P., E. Beucler, M. Drilleau, A. Mocquet, P. Lognonné, and W. B. Banerdt (2015), Verifying single-station seismic approaches using Earth-based data: Preparation for data return from the InSight mission to Mars, *Icarus*, *248*, 230–242, doi:10.1016/j.icarus.2014.10.035.
- Pappalardo, R. T., M. J. S. Belton, H. H. Breneman, M. H. Carr, C. R. Chapman, G. C. Collins, T. Denk, S. Fagents, P. E. Geissler, B. Giese, R. Greeley, R. Greenberg, J. W. Head, P. Helfenstein, G. Hoppa, S. D. Kadel, K. P. Klaasen, J. E. Klemazewski, K. Magee, A. S. McEwen, J. M. Moore, W. B. Moore, G. Neukum, C. B. Phillips, L. M. Prockter, G. Schubert, D. A. Senske, R. J. Sullivan, B. R. Tufts, E. P. Turtle, R. Wagner, and K. K. Williams (1999), Does Europa have a subsurface ocean? Evaluation of the geological evidence, *J. Geophys. Res.*, *104*(E10), 24,015–24,055, doi:10.1029/1998JE000628.
- Peters, L. E., S. Anandakrishnan, R. B. Alley, and D. E. Voigt (2012), Seismic attenuation in glacial ice: A proxy for englacial temperature, *J. Geophys. Res.*, *117*(F2), F02,008, doi:10.1029/2011JF002201.
- Peterson, J. (1993), Observation and modeling of background seismic noise, U.S. Geol. Surv. Open-File Rept. 92-322.
- Phillips, C. B., and R. T. Pappalardo (2014), Europa Clipper mission concept: Exploring Jupiter's ocean moon, *EOS Trans. Amer. Geophys. Union*, *95*(20), 165–167, doi:10.1002/2014EO200002.
- Pike, W. T., S. Calcutt, I. M. Standley, A. G. Mukherjee, J. Temple, T. Warren, C. Charalambous, H. Liu, A. Stott, and J. B. McClean (2016), A silicon seismic package (SSP) for planetary geophysics, in *47th Lunar and Planetary Science Conference*, p. Abstract # 2081, Lunar and Planetary Inst., Houston, TX.
- Rhie, J., and B. A. Romanowicz (2004), Excitation of Earth's continuous free oscillations by atmosphere-ocean-seafloor coupling, *Nature*, *431*, 552–556, doi:10.1038/nature02942.
- Rhoden, A. R., T. A. Hurford, L. Roth, and K. Retherford (2015), Linking Europa's plume activity to tides, tectonics, and liquid water, *Icarus*, *253*, 169–178.
- Ringler, A. T., and C. R. Hutt (2010), Self-noise models of seismic instruments, *Seis. Res. Lett.*, *81*(6), 972–983, doi:10.1785/gssrl.81.6.972.
- Rodgers, P. W. (1994), Self-noise spectra for 34 common electromagnetics seismometer/preamplifier pairs, *Bull. Seism. Soc. Am.*, *84*(1), 222–228.

- Roth, L., J. Saur, K. D. Retherford, D. F. Strobel, P. D. Feldman, M. A. McGrath, and F. Nimmo (2014), Transient water vapor at Europa's south pole, *Science*, *343*(6167), 171–174.
- Russell, C. (Ed.) (2012), *The Galileo Mission*, Springer Science + Business Media.
- Sato, H. (1982), Attenuation of S waves in the lithosphere due to scattering by its random velocity structure, *J. Geophys. Res.*, *87*, 7779–7785.
- Saygin, E., P. R. Cummins, and D. Lumley (2017), Retrieval of the P wave reflectivity response from autocorrelation of seismic noise: Jakarta Basin, Indonesia, *Geophys. Res. Lett.*, *44*(2), 792–799, doi:10.1002/2016GL071363.
- Schubert, G. J., J. Anderson, T. Spohn, and W. B. McKinnon (2004), Interior composition, structure and dynamics of the Galilean satellites, in *Jupiter: The planet, satellites and magnetosphere*, edited by F. Bagenal, T. E. Dowling, and W. B. McKinnon, chap. 13, pp. 281–306, Cambridge Univ. Press.
- Soderlund, K. M., B. E. Schmidt, J. Wicht, and D. D. Blankenship (2014), Ocean-driven heating of Europa's icy shell at low latitudes, *Nature Geoscience*, *7*, 16–19, doi:10.1038/ngeo2021.
- Sparks, W., B. Schmidt, M. McGrath, K. Hand, J. Spencer, M. Cracraft, and S. Deustua (2017), Active cryovolcanism on Europa?, *The Astrophysical Journal Letters*, *839*(2), L18.
- Stähler, S. C., M. P. Panning, S. D. Vance, M. van Driel, T. Nissen-Meyer, and S. Kedar (2017), Seismic wave propagation in icy ocean moons, *J. Geophys. Res.*, in preparation.
- Tibuleac, I. M., and D. von Seggern (2012), Crust-mantle boundary reflectors in Nevada from ambient noise autocorrelations, *Geophys. J. Int.*, *189*(1), 493–500, doi:10.1111/j.1365-246X.2011.05336.x.
- Tobie, G., G. Choblet, and C. Sotin (2003), Tidally heated convection: Constraints on Europa's ice shell thickness, *J. Geophys. Res.*, *108*(E11), doi:10.1029/2003JE002099.
- van Driel, M., L. Krischer, S. C. Stähler, K. Hosseini, and T. Nissen-Meyer (2015), Instantaneous global seismograms based on a broadband waveform database, *Solid Earth*, *6*, 701–717, doi:10.5194/se-6-701-2015.
- Vance, S., J. Harnmeijer, J. Kimura, H. Hussmann, B. Demartin, and J. M. Brown (2007), Hydrothermal systems in small ocean planets, *Astrobiology*, *7*(6), 987–1005, doi:10.1089/ast.2007.0075.
- Vance, S. D., M. Bouffard, M. Choukroun, and C. Sotin (2014), Ganymede's internal structure including thermodynamics of magnesium sulfate oceans in contact with ice, *Plan. & Space Sci.*, *96*, 62–70, doi:10.1016/j.pss.2014.03.011.
- Vance, S. D., S. Kedar, M. P. Panning, S. C. Stähler, B. G. Bills, R. D. Lorenz, H.-H. Huang, W. T. Pike, J. C. Castillo, P. Lognonné, V. C. Tsai, and A. R. Rhoden (2017a), Vital signs: Seismology of ocean worlds, *Astrobiology*, in revision.
- Vance, S. D., M. P. Panning, S. C. Stähler, B. G. Bills, F. Cammarano, V. Tsai, H.-H. Huang, S. Kedar, C. Sotin, W. B. Banerdt, S. Anandkrishnan, W. T. Pike, and R. Lorenz (2017b), Geophysical test for habitability in ocean worlds, *J. Geophys. Res.*, in preparation.
- Wang, T., X. Song, and H. H. Xia (2015), Equatorial anisotropy in the inner part of the Earth's inner core from autocorrelation of earthquake coda, *Nature Geoscience*, *8*, 224–227, doi:10.1038/ngeo2354.
- Williams, J. G., D. H. Boggs, C. F. Yoder, J. T. Ratcliff, and J. O. Dickey (2001), Lunar rotational dissipation in solid body and molten core, *J. Geophys. Res.*, *106*(E11), 27,933–27,968, doi:10.1029/2000JE001396.
- Zahnle, K., P. Schenk, H. Levison, and L. Dones (2003), Cratering rates in the outer solar system, *Icarus*, *163*, 263–289, doi:10.1016/S0019-1035(03)00048-4.
- Zhan, Z., V. C. Tsai, J. M. Jackson, and D. Helmberger (2013), Ambient noise correlation on the Amery Ice Shelf, East Antarctica, *Geophys. J. Int.*, *196*, 1796–1802, doi:10.1093/gji/ggt488.
- Zhu, P., G. E. Manucharyan, A. F. Thompson, J. C. Goodman, and S. D. Vance (2017), The influence of a freshwater layer on Europa's overturning circulation, *Geophys. Res. Lett.*, submitted.